Supporting Information for

Moisture-tolerant and high-quality α-$CsPbI_3$ films for efficient and stable perovskite solar modules

Ruihao Chen,[a] Yong Hui,[b] Binghui Wu,[a] Yongke Wang,[b] Xiaofeng Huang,[b] Zhongyuan Xu,[a] Pengpeng Ruan,[b] Wuyong Zhang,[b] Fangwen Cheng,[b] Weijie Zhang,[b] Jun Yin,*[a] Jing Li*[a] and Nanfeng Zheng*[b]

[a] Collaborative Innovation Center for Optoelectronic Semiconductors and Efficient Devices, Pen-Tung Sah Institute of Micro-Nano Science and Technology, Xiamen University, Xiamen 361005, China.

[b] State Key Laboratory for Physical Chemistry of Solid Surfaces, Collaborative Innovation Center of Chemistry for Energy Materials, National & Local Joint Engineering Research Center of Preparation Technology of Nanomaterials, College of Chemistry and Chemical Engineering, Xiamen University, Xiamen 361005, China.

* Corresponding authors.

E-mails: jyin@xmu.edu.cn (J. Yin), lijing@xmu.edu.cn (J. Li); nfzheng@xmu.edu.cn (N. F. Zheng)

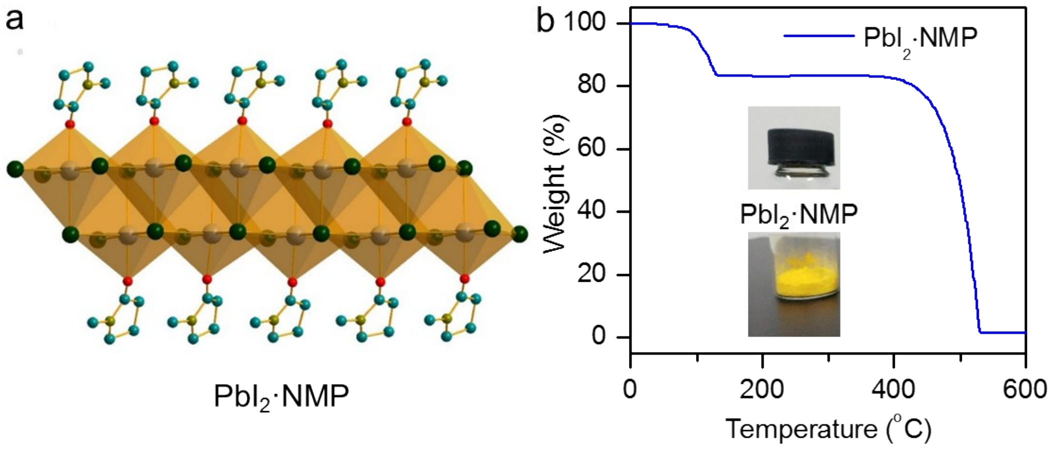

Figure S1. (a) Crystal structure [1] and (b) TG analysis of the PbI_2·NMP compound. Inset shows the photograph of the corresponding crystal powders. Obviously, the color of PbI_2·NMP compound is different from pristine PbI_2 powder (purchased from Alfa Aesar).

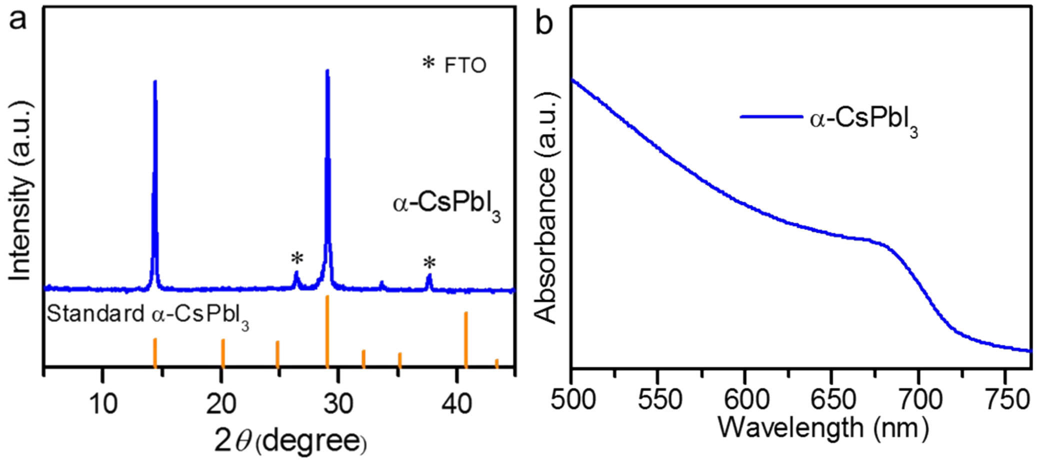

Figure S2. (a) XRD patterns and (b) UV-vis spectrum of $CsPbI_3$ film produced from PbI_2·NMP compound.

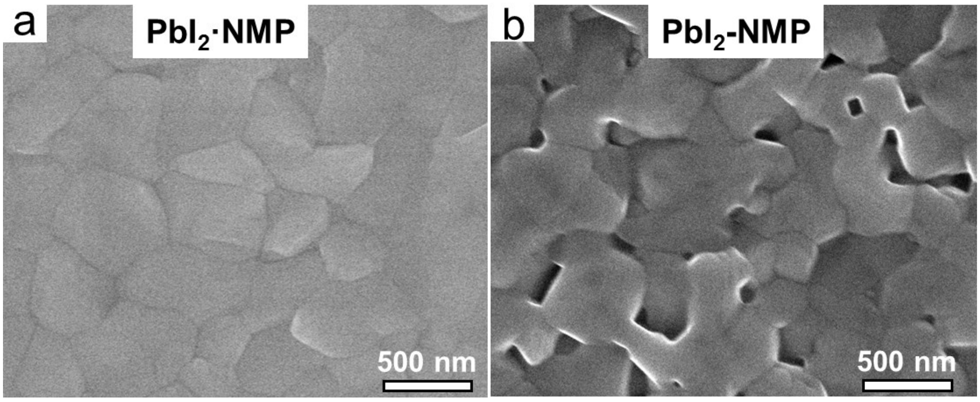

Figure S3. Top-view SEM images of $CsPbI_3$ films derived from (a) PbI_2·NMP compound and (b) NMP-doped precursor (PbI_2-NMP). It can be seen that PbI_2·NMP compound have effectively improved the reproducibility and uniformity of $CsPbI_3$ film.

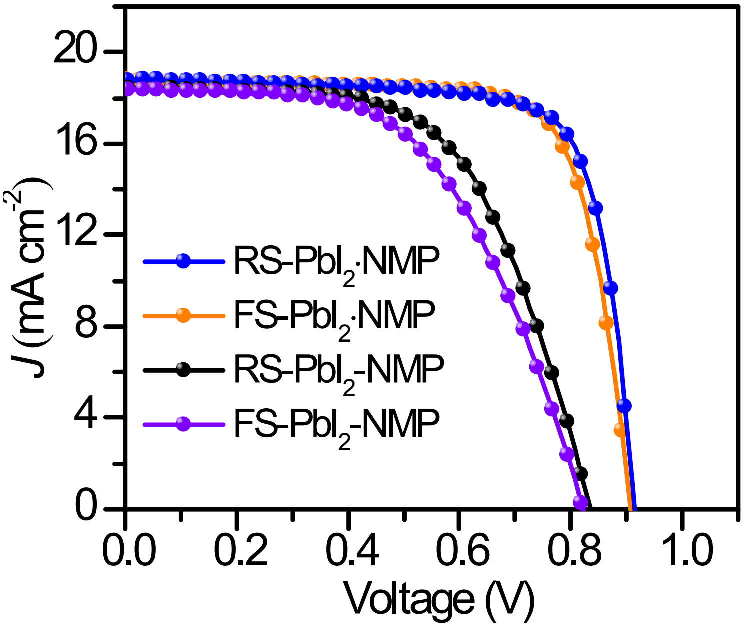

Figure S4. *J-V* curves of champion PSCs based on $CsPbI_3$ films from PbI_2·NMP compound or NMP-doped precursor (PbI_2-NMP). Considering the acylamino groups can interact with Cs^+ ions, and induce electron cloud density enhancement on the surface of $CsPbI_3$ which is beneficial for the PV performance improvement of PSCs,[2] the acylamino groups of NMP from PbI_2·NMP complex was utilized. PbI_2·NMP complex could effectively supply more binding sites than the precursor mixture solution (NMP as an additive) to facilitate the $CsPbI_3$ film growth. Thus, PbI_2·NMP complex could effectively improve the density of $CsPbI_3$ film, and the corresponding devices have higher PCE.

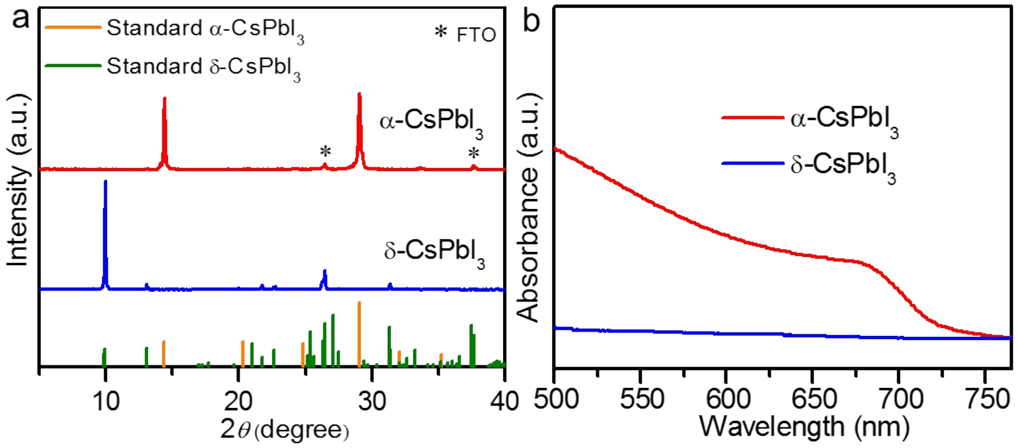

Figure S5. (a) XRD patterns and (b) UV-vis spectra of α-$CsPbI_3$ and δ-$CsPbI_3$ films for a comparison.

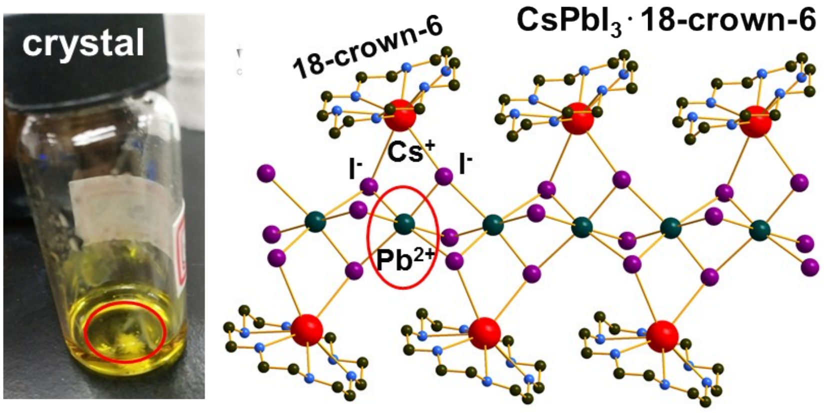

Figure S6. Photograph image and molecular structure of $CsPbI_3 \cdot$18-crown-6 crystal. (Cs red, Pb dark green, I purple, C black, O light blue). Hydrogen atoms are omitted for clarity. In this work, a needle-like crystal structure analogue, $CsPbI_3 \cdot$18-crown-6, was first synthesized and determined by single-crystal X-ray diffraction. The framework of $CsPbI_3 \cdot$18-crown-6 crystal consists of 18-crown-6 capped Cs^+ and a chain (PbI_3^-). The result strongly verified the interaction of 18-crown-6 and Cs^+ ion.

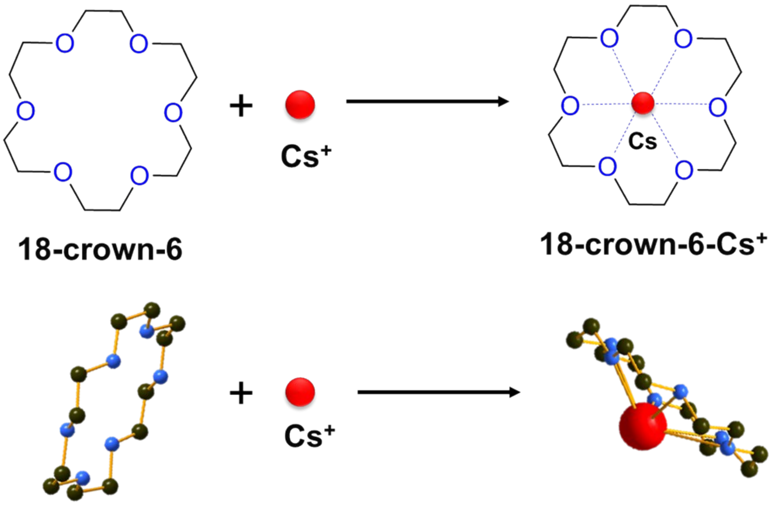

Figure S7. The chelation structure of 18-crown-6, Cs^+ and 18-crown-6-Cs^+. (Cs red, C black, O light blue). Hydrogen atoms are omitted for clarity.

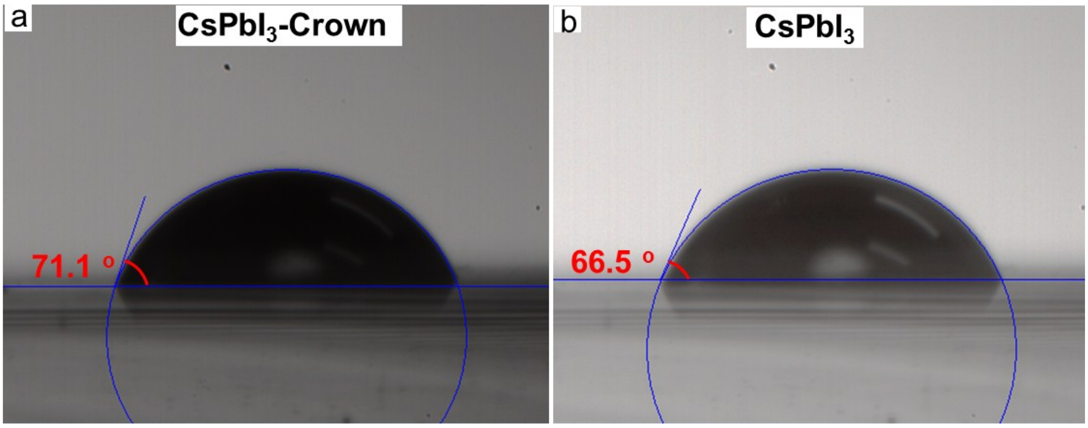

Figure S8. The images of water contact angles measured on (a) the $CsPbI_3$-Crown film compared to (b) that on a $CsPbI_3$ film.

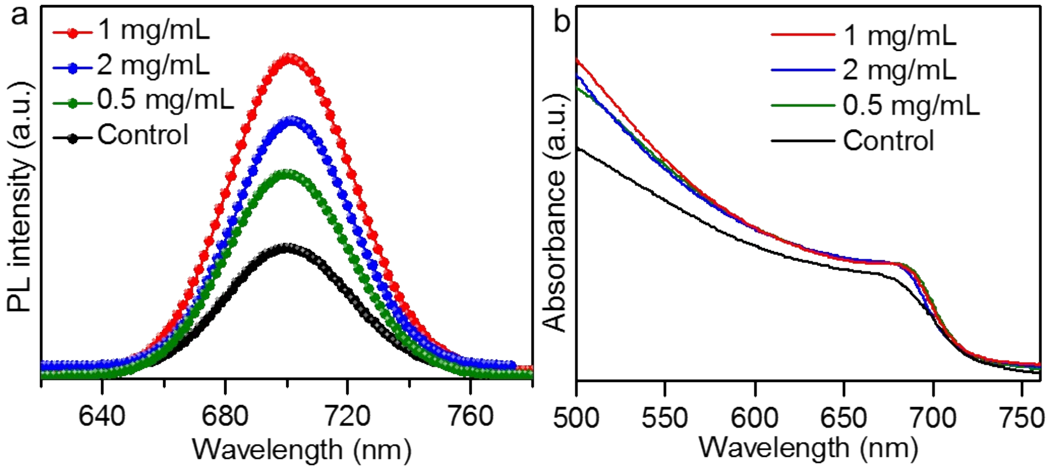

Figure S9. (a) PL and (b) UV-vis spectra of the $CsPbI_3$-Crown films produced with Crown in different concentrations with the comparison to those of the control ($CsPbI_3$) film.

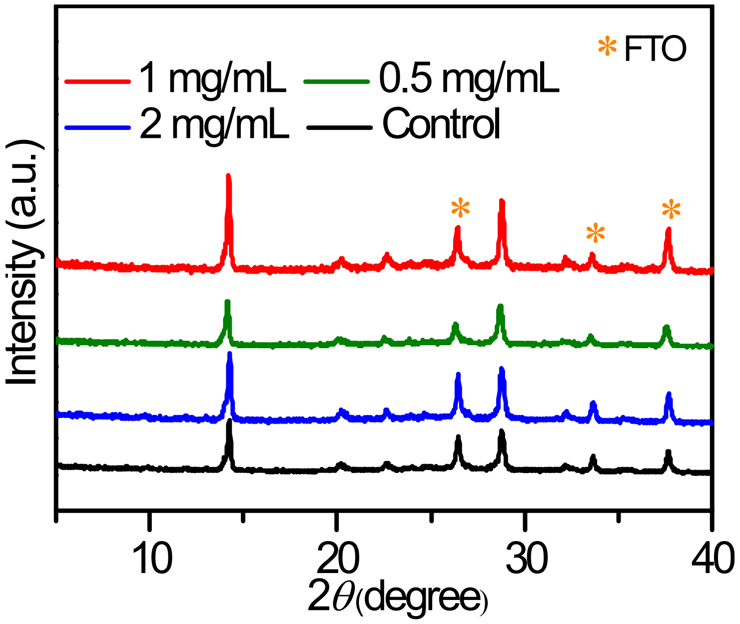

Figure S10. XRD patterns of $CsPbI_3$-Crown films produced with Crown in different concentrations with the comparison to that of the control ($CsPbI_3$) film.

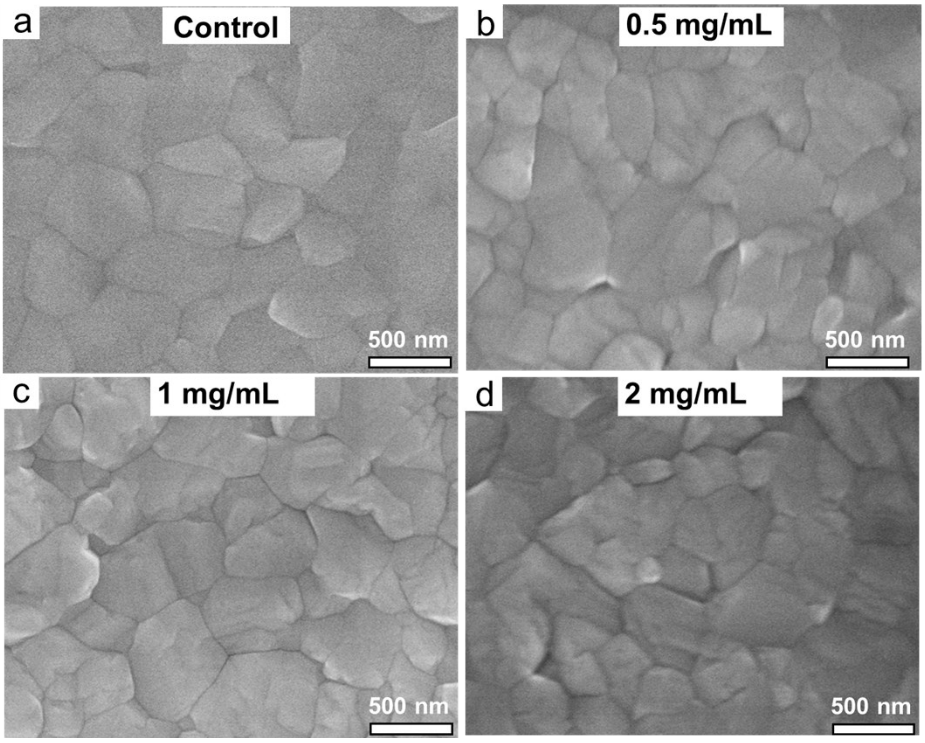

Figure S11. SEM images of the $CsPbI_3$-Crown films produced with Crown in different concentrations with the comparison to that of the control ($CsPbI_3$) film.

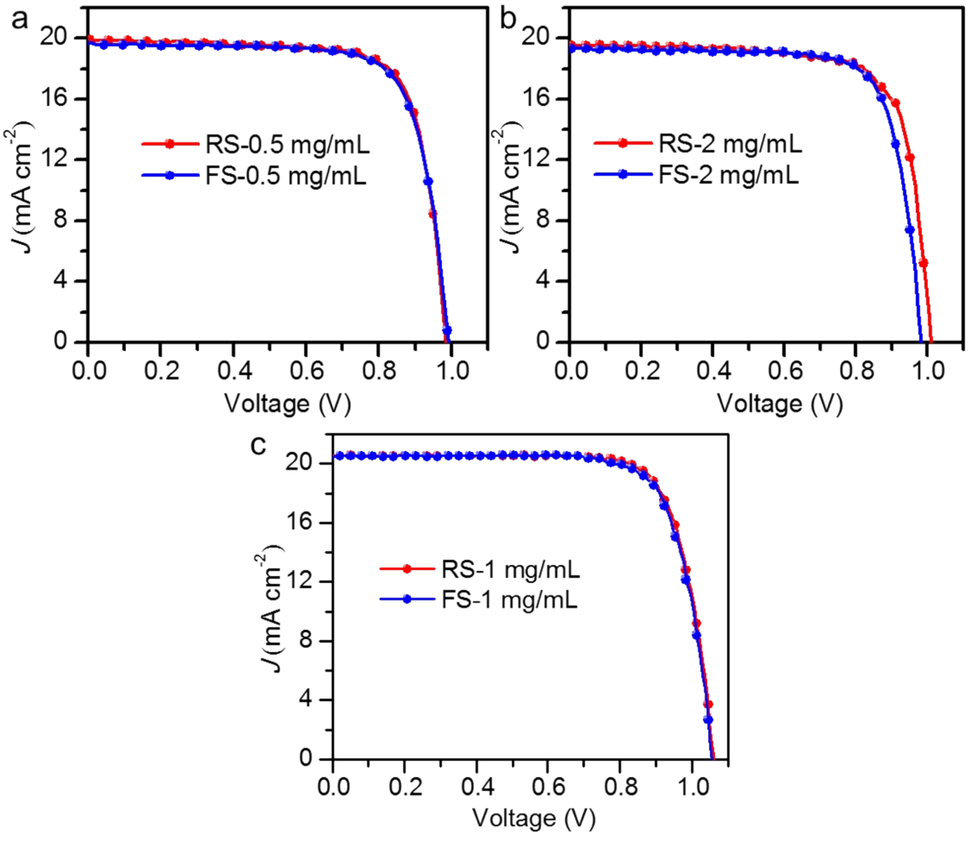

Figure S12. *J-V* curves of champion PSCs based on $CsPbI_3$-Crown films produced with Crown in different concentrations. Here, it is understandable that the small amount of crown ether would lead to the insufficient modification of perovskites, resulting the less improvement in photovoltaic performance. However, the excess crown ether mightily act as additional defect centers located at the interface, resulting the decreased device performance.

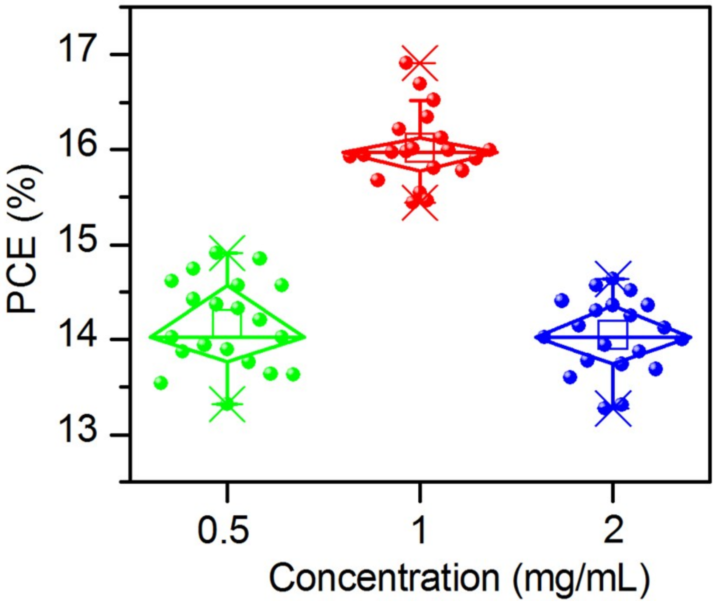

Figure S13. PCE statistics of 20 individual PSCs based on $CsPbI_3$-Crown films produced with Crown in different concentrations.

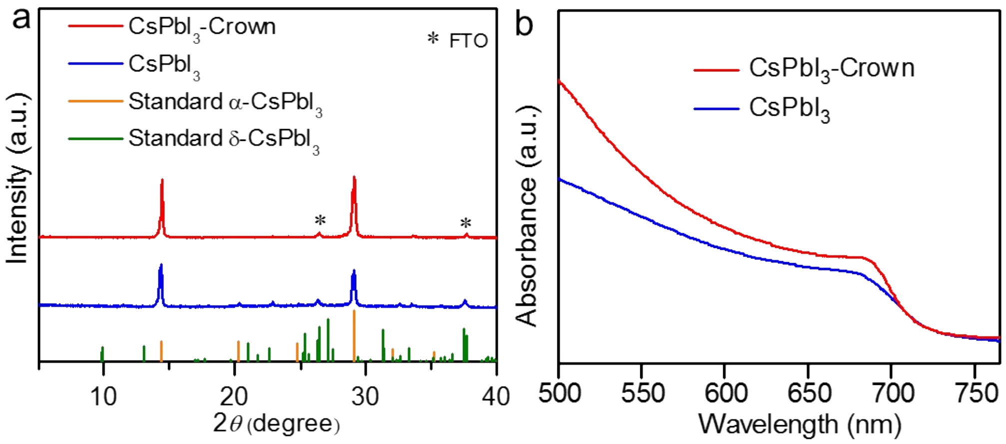

Figure S14. (a) XRD patterns and (b) UV-vis spectra of $CsPbI_3$-Crown films with the comparison to those of the $CsPbI_3$ films.

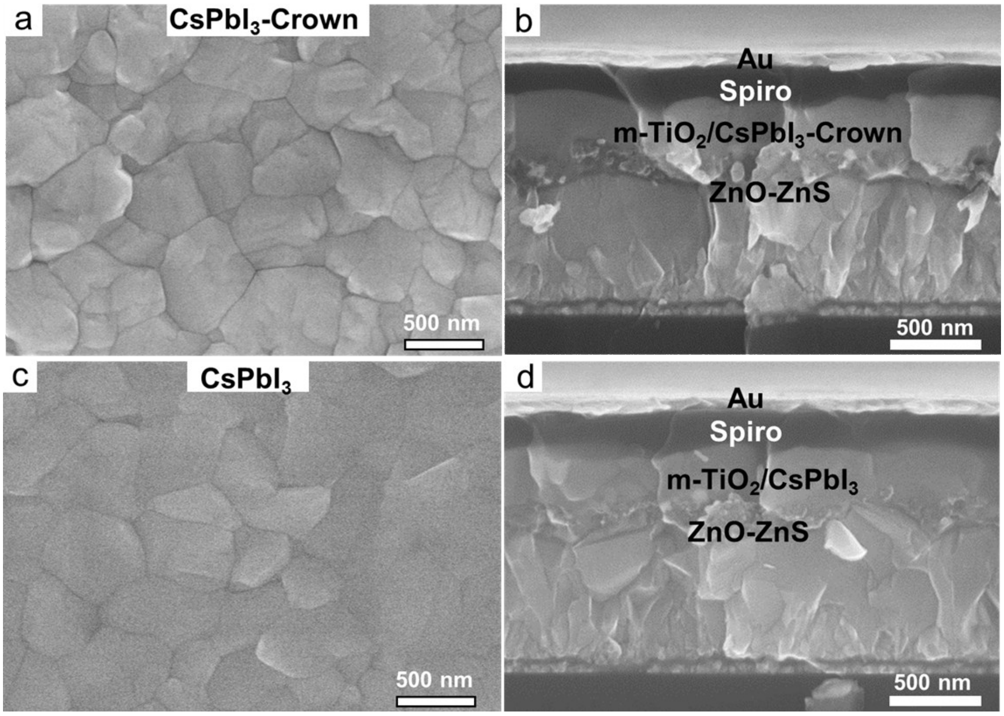

Figure S15. Top-view and cross-sectional SEM images of (a, b) CsPbI$_3$-Crown films compared to (c, d) CsPbI$_3$ films in devices.

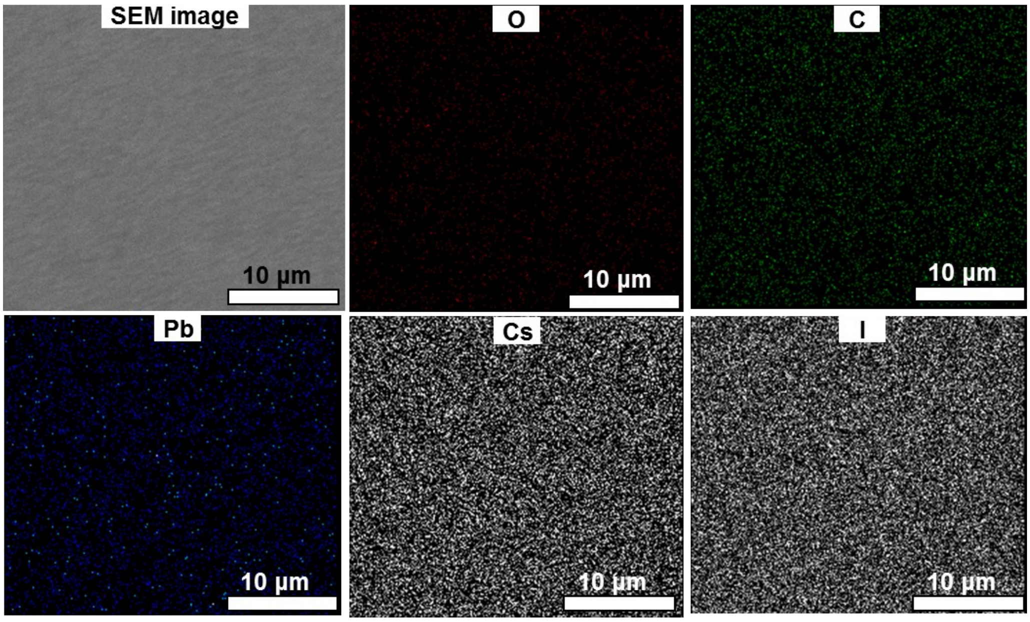

Figure S16. The SEM image and elemental maps of the CsPbI$_3$-Crown film.

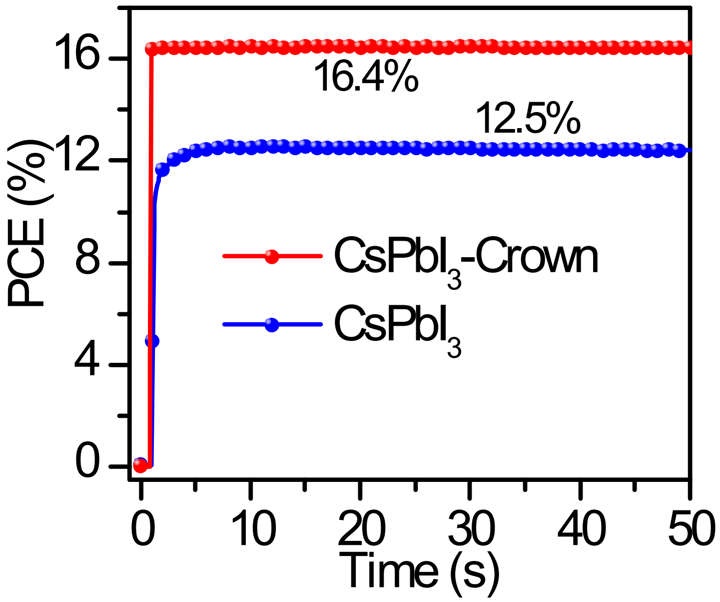

Figure S17. Steady-state PCE of the CsPbI$_3$-Crown device compared with that of CsPbI$_3$ PSC measured at V_{bias} of 0.90 and 0.77 V, respectively.

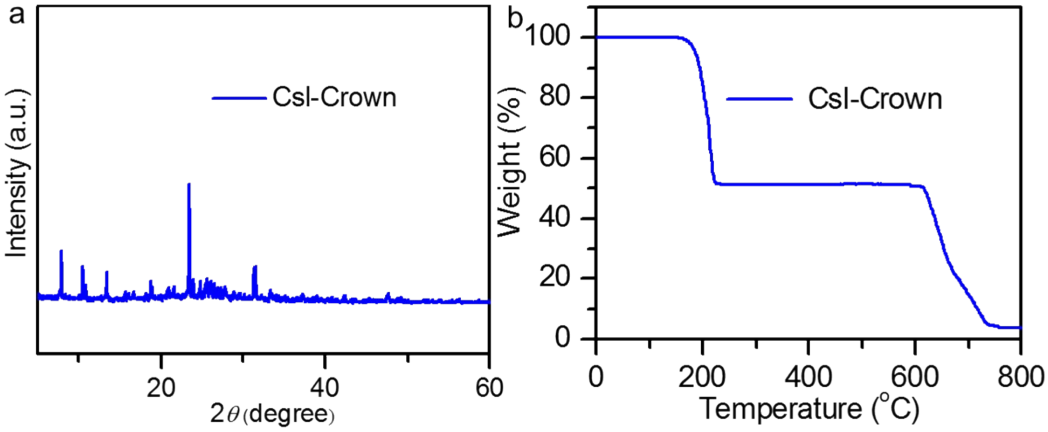

Figure S18. (a) XRD pattern and (b) TG analysis of CsI-Crown compound. The results demonstrated that CsI-Crown is very stable due to the strong interaction between Cs$^+$ from CsI and O atom of Crown.

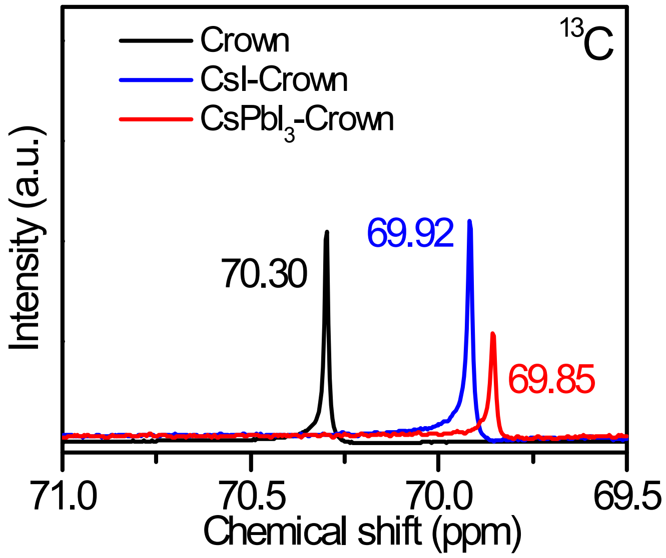

Figure S19. ${}^{13}C$ liquid-state NMR spectra of $CsPbI_3$-Crown solution dissolved with DMSO-d_6 with the Crown and CsI-Crown solutions as references. ${}^{13}C$ NMR spectra showed the resonance signal of $\delta = 70.3$ ppm belonging to CH_2 group underwent significantly upfield shifts of $\Delta\delta = 0.38, 0.45$ ppm due to the interaction of Crown with CsI and $CsPbI_3$, respectively.

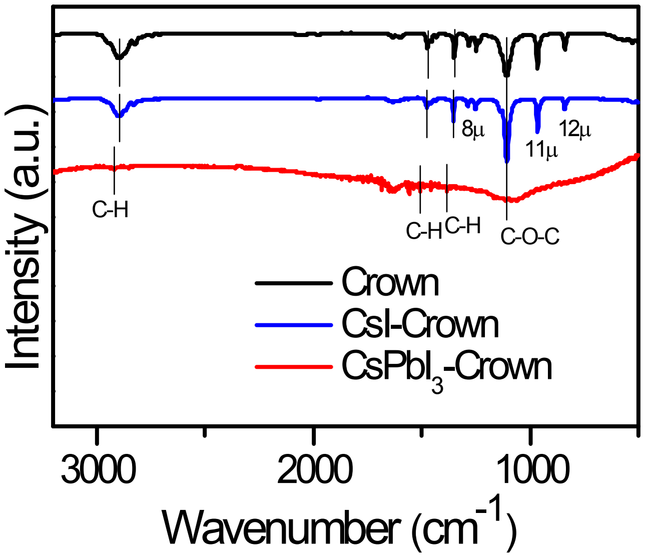

Figure S20. IR spectrum of $CsPbI_3$-Crown with the spectra of Crown and CsI-Crown as references. The IR spectrum of pure Crown displayed absorption bands in region of 1473 and 1348 cm^{-1} which are attributed to the typical functional groups of C-H bending vibration of Crown. With the incorporation of $CsPbI_3$ and CsI, the corresponding vibration modes shifted. The stronger interaction between O atom of Crown and Cs^+ of $CsPbI_3$ or CsI resulted in a shift in the vibrational wavenumber.

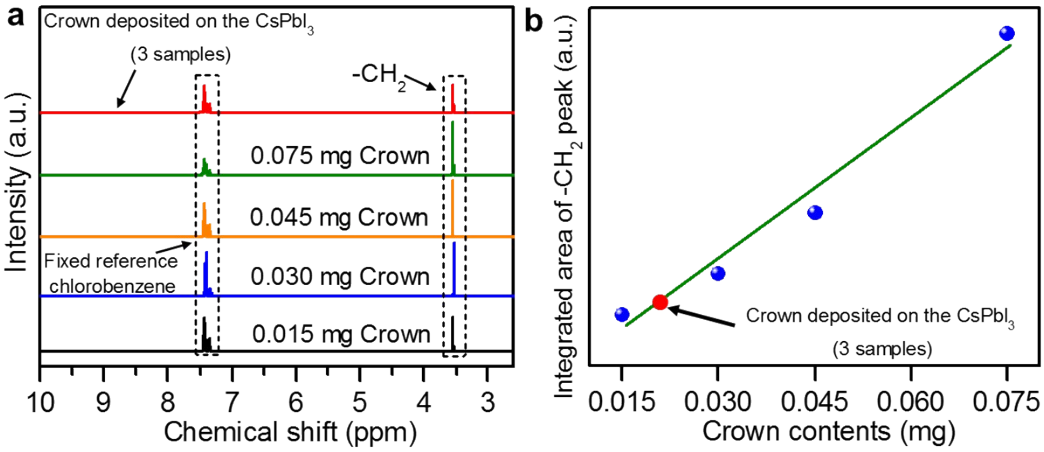

Figure S21. (a) ^{1}H NMR of different Crown contents and the Crown signal from three samples of $CsPbI_3$-Crown films, which were dissolved in DMSO-d_6. The fixed chlorobenzene content was regarded as calibration reference. (b) Relationship between integrated area (-CH_2 peak from Crown) and Crown contents. The Crown content of three samples $CsPbI_3$-Crown films is about ~0.021 mg. Each $CsPbI_3$-Crown film contains Crown about 0.007 mg corresponding to ~1 weight % with respect to $CsPbI_3$.

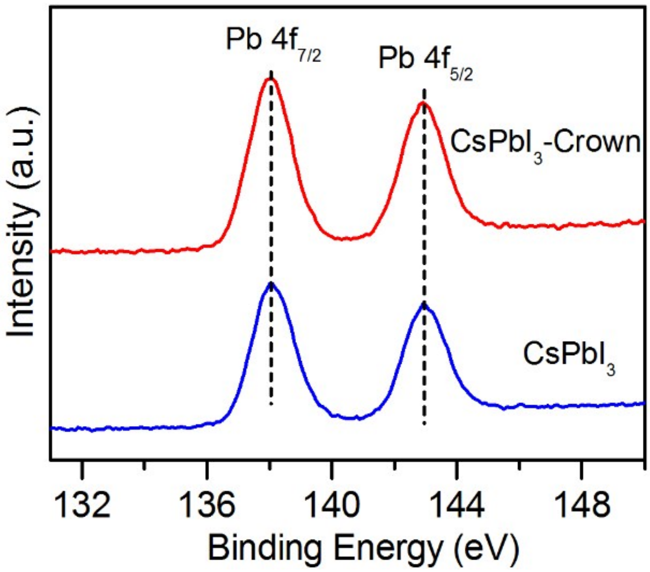

Figure S22. Pb 4f XPS spectra of $CsPbI_3$-Crown and $CsPbI_3$ films.

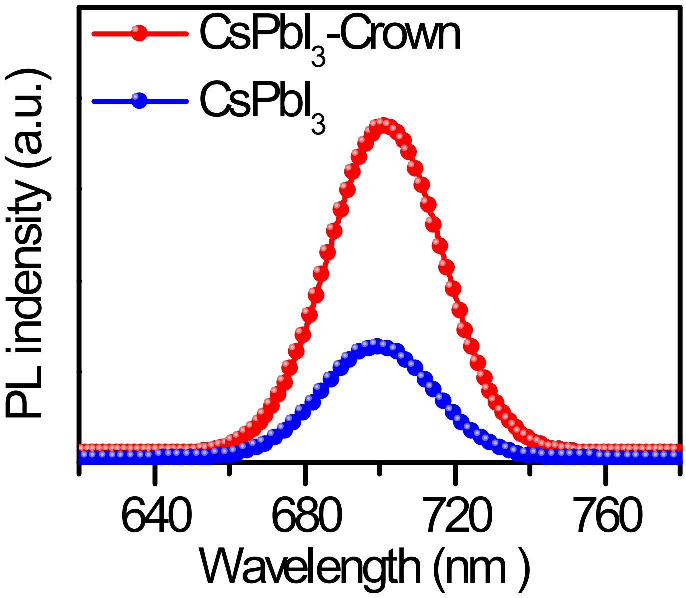

Figure S23. Steady-state PL spectra of CsPbI$_3$-Crown and CsPbI$_3$ films deposited on glass substrates. The excitation wavelength was set as 377.6 nm with filter chip.

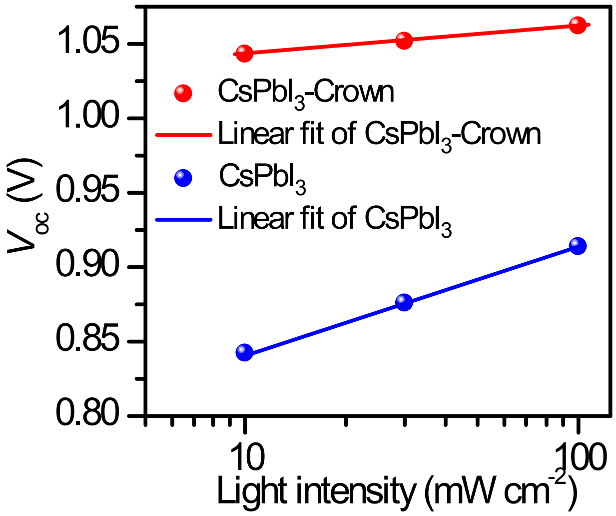

Figure S24. Light intensity dependent V_{oc} in CsPbI$_3$-Crown devices compared with that of CsPbI$_3$ PSCs. The fitting line gave a slope of nk_BT/q, where n, k_B, T, and q are the ideality factor, Boltzmann constant, absolute temperature, and elementary charge, respectively.

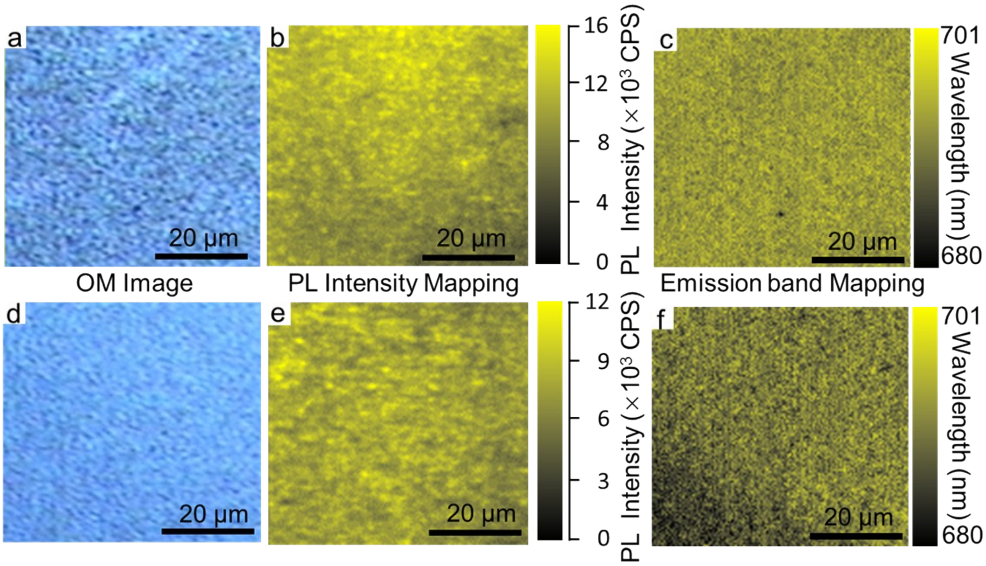

Figure S25. OM images, the corresponding PL mapping and emission band mapping of the (a-c) $CsPbI_3$-Crown films with the comparisons to those in $CsPbI_3$ films (d-f).

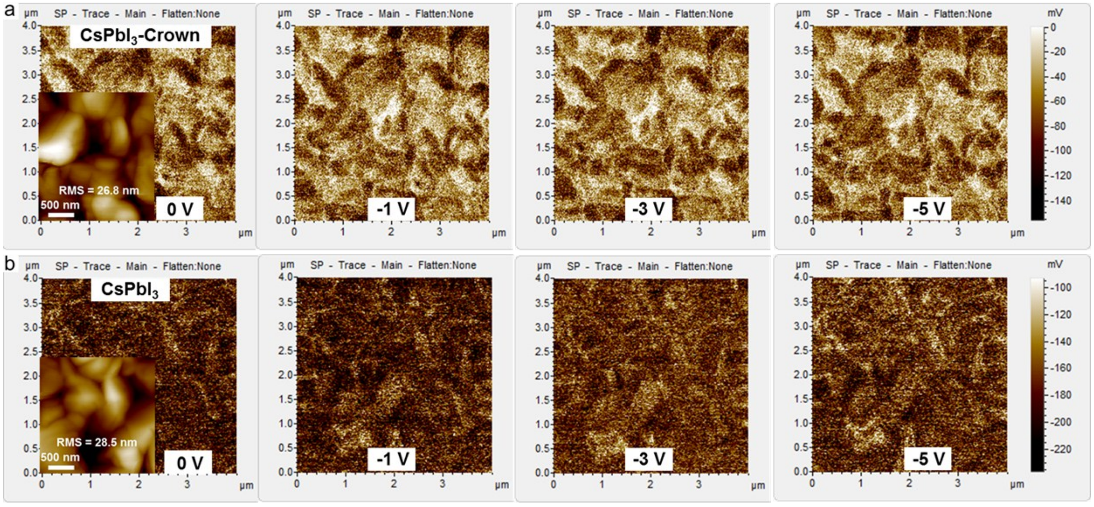

Figure S26. Surface potential (SP) images of (a) $CsPbI_3$-Crown compared to those of (b) $CsPbI_3$ films at different bias voltages applied to the tip under dark condition. Insets are the corresponding topography images. As in the results, there is no obvious discrepancies in the morphology and surface roughness in the $CsPbI_3$-Crown film with a root-mean-square roughnesses (RMS) of 26.8 nm compared to 28.5 nm in the $CsPbI_3$ film. The homogeneous contrast of SP images indicated the uniform SP in both $CsPbI_3$-Crown and $CsPbI_3$ films. While, with decreasing the bias voltage at the tip from 0 V to -5 V, no obvious change can be observed in the $CsPbI_3$-Crown film with contrast to the more and brighter SP images in the $CsPbI_3$ film. These results demonstrated that Crown passivation could effectively enhance the physical stability of $CsPbI_3$ perovskites under the electric-field driving by inhibiting the surface ion migration on the $CsPbI_3$.

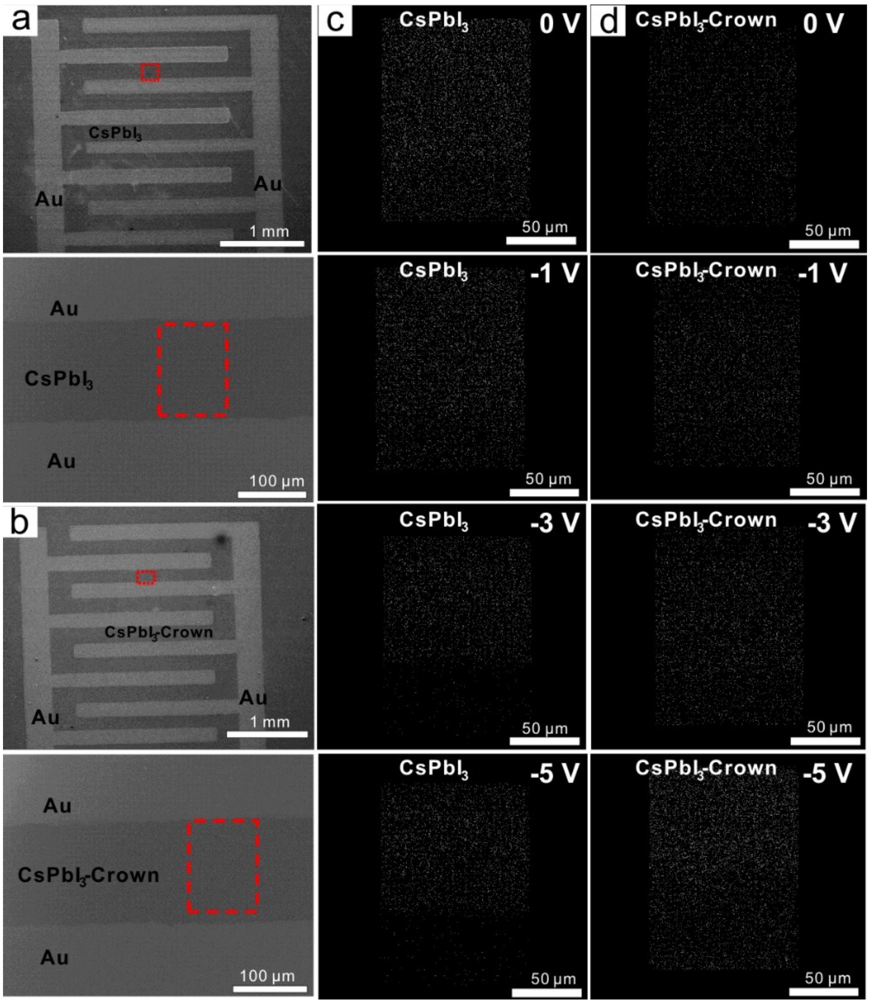

Figure S27. Evaluation of the ions migration under electric-field driving by the EDS mapping for the $CsPbI_3$ films. (a) and (b) show the co-plane devices with interdigital electrodes on $CsPbI_3$ and $CsPbI_3$-Crown films, respectively. Red dotted rectangle represents the test region. The typical Cs element mapping of (c) $CsPbI_3$-Crown and (d) $CsPbI_3$ films at different bias voltages (from 0 V to -5 V) were representatively shown in the figure.

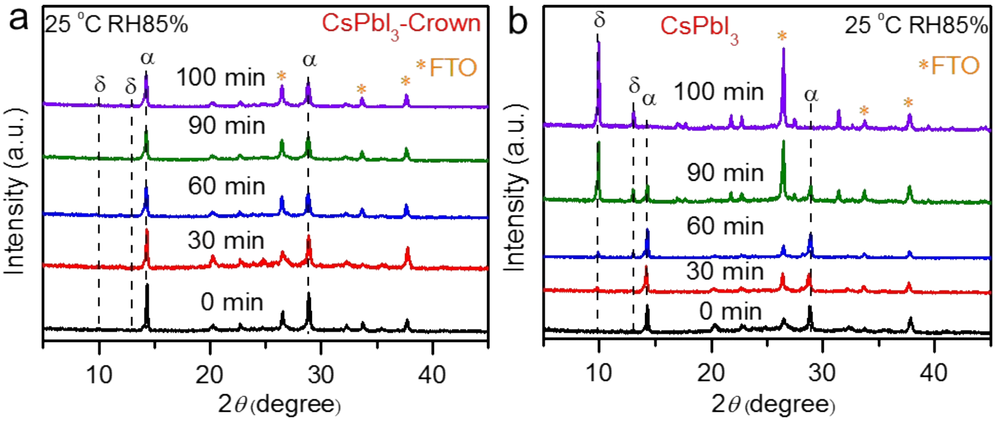

Figure S28. XRD patterns of (a) $CsPbI_3$-Crown and (b) $CsPbI_3$ films in ambient atmosphere (25 °C) at RH 85% with different aging time.

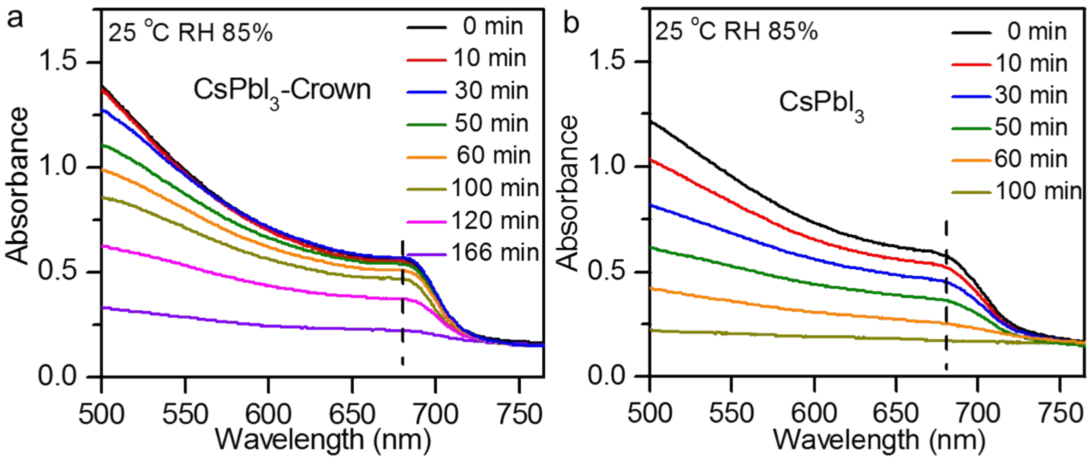

Figure S29. The UV-vis spectra of (a) $CsPbI_3$-Crown film compared to those of (b) $CsPbI_3$ film accelerated aging in ambient atmosphere (25 °C) at RH 85% with different aging time.

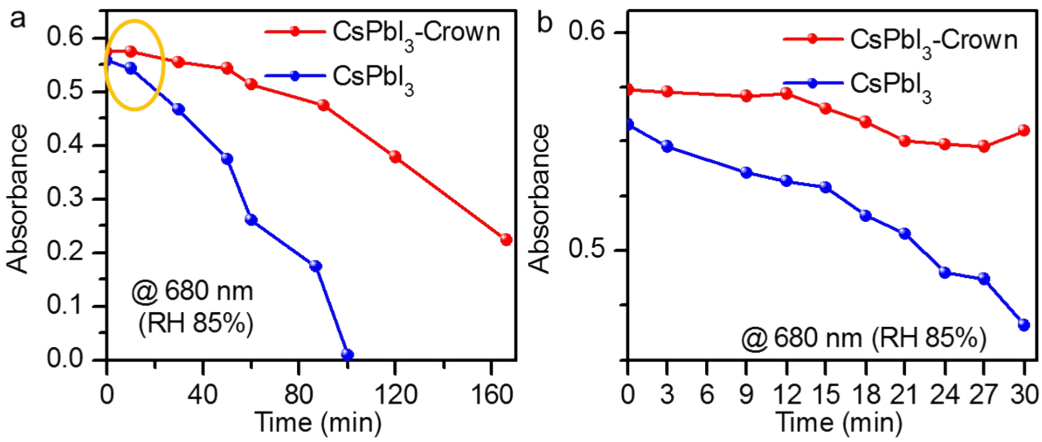

Figure S30. The absorbance variation of (a) the CsPbI$_3$-Crown and CsPbI$_3$ films with the data extracted from Figure S29 at the wavelength of 680 nm, and (b) the zoomed-in curves from the orange circle marked in (a). The intensity of absorbance of CsPbI$_3$-Crown films slightly decreased along time variation, while CsPbI$_3$ totally transformed to yellow δ phase within 100 min.

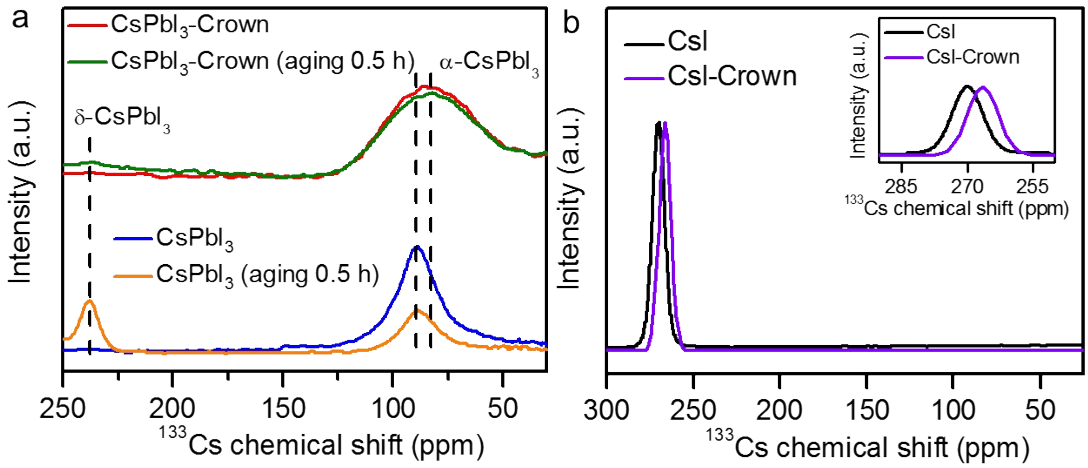

Figure S31. ^{133}Cs solid-state MAS NMR spectra of (a) CsPbI$_3$-Crown and CsPbI$_3$ before and after aging for 0.5 h at RH 85%, (b) CsI and CsI-Crown powders at 12 kHz MAS and 298 K. Inset is the corresponding amplified spectrum. As in the results, the characteristic peak centered at ~240 ppm belongs to the ^{133}Cs of δ-CsPbI$_3$.[3] The peak centered at 89.4 ppm should be assigned to the ^{133}Cs of α-CsPbI$_3$. After Crown was introduced on CsPbI$_3$ surface, the center of ^{133}Cs peak was shifted to 83.8 ppm and much broader due to the interaction of Crown and CsPbI$_3$. The ^{133}Cs peak intensity of α-$CsPbI_3$ was not obviously changed on the $CsPbI_3$-Crown, but evidently weaken in the $CsPbI_3$ after aging for 0.5 h. Moreover, the $CsPbI_3$ was partially degraded to the δ-$CsPbI_3$, while the $CsPbI_3$-Crown was more stable after aging for 0.5 h. The ^{133}Cs peak of cesium iodide was also shifted after Crown passivation. The above results indicated that Crown effectively inhibited the moisture invasion and further improved the phase stability of $CsPbI_3$ films.

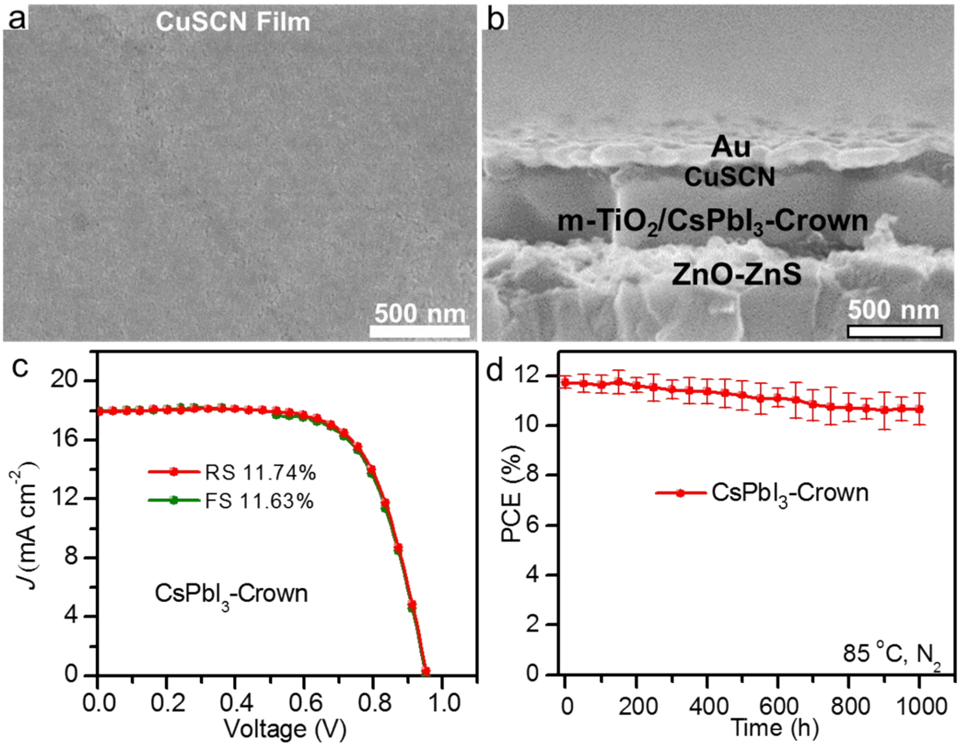

Figure S32. (a)The top-view SEM image of the CuSCN film. (b) The cross-section SEM image of the $CsPbI_3$-Crown PSC based on CuSCN film as HTL. (c) *J-V* curve of the champion cell based on $CsPbI_3$-Crown film using CuSCN as HTL. (d) Operation stability of $CsPbI_3$-Crown devices measured at 85 °C in N_2 atmosphere. Error bars represent the standard error.

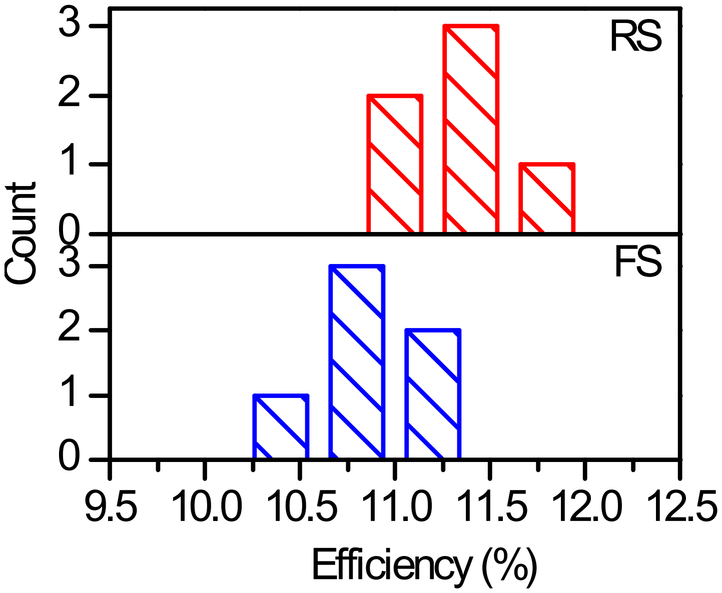

Figure S33. RS and FS mode-efficiency distribution in 6 individual $CsPbI_3$-Crown PSC modules by spin coating method.

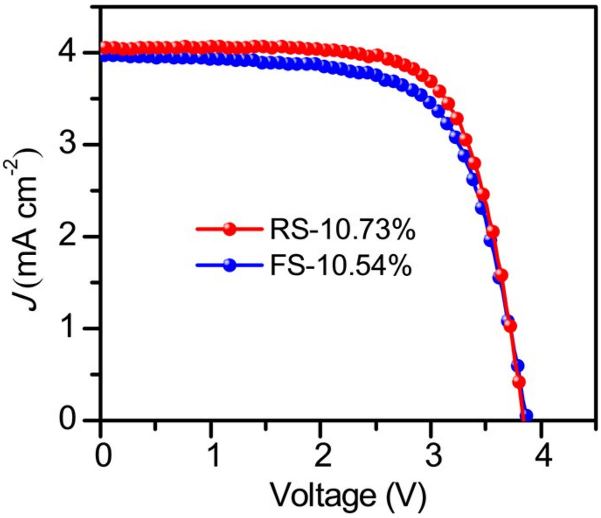

Figure S34. *J-V* curves of the $CsPbI_3$-Crown based champion PSC module fabricated by blade coating method.

Table S1. Photovoltaic parameters of the champion efficiency for $CsPbI_3$ PSCs derived from PbI_2·NMP and PbI_2-NMP.

Device		J_{sc}/mA·cm^{-2}	V_{oc}/V	FF/%	η/%
PbI_2·NMP	Reverse	18.73	0.89	75.19	12.53
	Forward	18.81	0.91	76.13	13.03
PbI_2-NMP	Reverse	18.41	0.83	60.50	9.24
	Forward	18.37	0.82	55.51	8.36

Table S2. Photovoltaic parameters of $CsPbI_3$-Crown PSCs with different concentrations of Crown.

Device		J_{sc}/mA·cm^{-2}	V_{oc}/V	FF/%	η/%
0.5 mg mL^{-1}	Reverse	19.89	0.99	76.11	14.91
	Forward	19.60	0.99	75.65	14.73
1 mg mL^{-1}	Reverse	20.56	1.06	77.61	16.91
	Forward	20.51	1.05	77.12	16.76
2 mg mL^{-1}	Reverse	19.52	1.01	74.90	14.74
	Forward	19.32	0.98	76.68	14.55

Table S3. Photovoltaic parameters of the champion efficiency of $CsPbI_3$-Crown PSCs compared with $CsPbI_3$ PSCs.

Device		J_{sc}/mA·cm^{-2}	V_{oc}/V	FF/%	η/%
$CsPbI_3$	Reverse	18.73	0.89	75.19	12.53
	Forward	18.81	0.91	76.13	13.03
$CsPbI_3$-Crown	Reverse	20.56	1.06	77.61	16.91
	Forward	20.51	1.05	77.12	16.76

Table S4. The average efficiencies of $CsPbI_3$-Crown PSCs compared with $CsPbI_3$ PSCs.

Device		Average PCE%
$CsPbI_3$	Reverse	15.8±0.9
	Forward	15.6±1.0
$CsPbI_3$-Crown	Reverse	11.7±1.07
	Forward	11.1±1.4

Table S5. Photovoltaic parameters of the champion efficiency for $CsPbI_3$-Crown PSC based on CuSCN HTL.

Device		J_{sc}/mA·cm^{-2}	V_{oc}/V	*FF*/%	η/%
$CsPbI_3$-Crown	Reverse	17.93	0.95	68.90	11.74
	Forward	17.98	0.95	68.11	11.63

Table S6. Photovoltaic parameters of the champion efficiency of $CsPbI_3$-Crown PSCs module (active area of 8 cm^2).

Device		J_{sc}/mA·cm^{-2}	V_{oc}/V	*FF*/%	η/%
Spin coating	Reverse	4.10	4.05	71.45	11.87
	Forward	4.01	4.00	70.32	11.25
Blade coating	Reverse	4.05	3.84	69.02	10.73
	Forward	3.98	3.86	68.60	10.54

Table S7. Comparison of our device with published $CsPbI_3$-based PSCs.

Encapsulation Or not	Active area (cm^2)	Initial PCE (%)	Aging condition			Aging time (h)	% of Initial PCE after aging Time	Reference	Acceptation date
			Test condition	Testing atmosphere	Testing temperature (^{o}C)				
Not	0.10	16.91	Dark	Air, 20%	25	2000	90%	This work	
Not	0.10	11.74	Dark	N_2	85	1000	91%		
Yes	8.00	11.87	MPP	Air, 60%	25	515	95%		
Not	0.12	18.40	Dark	Air, <10%	RT	500	No decay	[4]	09-07-2019
Not			MPP	N_2		500	92%		
Not	0.12	16.62	Dark	Air, 10±5%	20-25	720	No decay	[5]	20-09-2019
Not	0.07	14.10	Dark	N_2	RT	168	87%	[6]	23-06-2019
Not	0.11	15.71	Dark	Air, 20-30%	25	1440	92%	[7]	26-09-2018
Not	0.11	15.07	Light soaking	N_2	25	500	98%	[8]	17-03-2018
Not	0.09	10.74	Dark	Air, 45-55%	RT	500	75%	[2]	25-01-2018
				N_2	60	500	80%		
Not	0.10	10.77	Dark	15-25%	RT	720	No decay	[9]	07-09-2016

RT represents room temperature.

MPP represents maximum power point tracking.

References

[1] F. Cheng, X. Jing, R. Chen, J. Cao, J. Yan, Y. Wu, X. Huang, B. Wu, N. F. Zheng, Inorg. Chem. Front. 2019, 6, 2458.

[2] B. Li, Y. Zhang, L. Fu, T. Yu, S. Zhou, L. Zhang, L. Yin, Nat. Commun. 2018, 9, 1076.

[3] D. J. Kubicki, D. Prochowicz, A. Hofstetter, S. M. Zakeeruddin, M. Gratzel, L. Emsley, J. Am. Chem. Soc. 2017, 139, 14173.

[4] Y. Wang, M. I. Dar, L. K. Ono, T. Zhang, M. Kan, Y. Li, L. Zhang, X. Wang, Y. Yang, X. Gao, Y. Qi, M. Grätzel, Y. Zhao, Science 2019, 365, 591.

[5] Y. Wang, X. Liu, T. Zhang, X. Wang, M. Kan, J. Shi, Y. Zhao, Angew. Chem. Int. Ed. 2019, 58, 16691.

[6] X. Ling, S. Zhou, J. Yuan, J. Shi, Y. Qian, B. W. Larson, Q. Zhao, C. Qin, F. Li, G. Shi, C. Stewart, J. Hu, X. Zhang, J. M. Luther, S. Duhm, W. Ma, Adv. Energy Mater. 2019, 9, 1900721.

[7] P. Wang, X. Zhang, Y. Zhou, Q. Jiang, Q. Ye, Z. Chu, X. Li, X. Yang, Z. Yin, J. You, Nat. Commun. 2018, 9, 2225.

[8] K. Wang, Z. Jin, L. Liang, H. Bian, D. Bai, H. Wang, J. Zhang, Q. Wang, L. Shengzhong, Nat. Commun. 2018, 9, 4544.

[9] A. Swarnkar, A. R. Marshall, E. M. Sanehira, B. D. Chernomordik, D. T. Moore, J. A. Christians, T. Chakrabarti, J. M. Luther, Science 2016, 354, 92.